Geosphere

Behavior of methane seep bubbles over a pockmark on the Cascadia continental margin

Marie S. Salmi, H. Paul Johnson, Ira Leifer and Julie E. Keister

Geosphere 2011;7;1273-1283
doi: 10.1130/GES00648.1

Notes

Behavior of methane seep bubbles over a pockmark on the Cascadia continental margin

Marie S. Salmi[1,*], H. Paul Johnson[1], Ira Leifer[2], and Julie E. Keister[1]
[1]*University of Washington, Seattle, Washington, 98195, USA*
[2]*University of California, Santa Barbara, California 93117, USA*

ABSTRACT

A newly modified acoustic method was used to derive time-dependent bubble emission size distributions and to monitor associated zooplankton behavior at a methane seep emitted from the northeast Pacific continental shelf in 150 m water depth near Grays Harbor, Washington State, USA. Instrumentation consisted of a seafloor mooring with an upward-oriented 200 kHz sonar that imaged the column's lower 100 m for 33 h during September 2009. The profiler observed several highly variable methane bubble streams venting from a large carbonate-lined pockmark. Other acoustic data and visual observations confirmed that the gas bubbles reached the sea surface and were highly variable in nature. Individual bubble traces in the acoustic sonar images were used to derive vertical bubble velocities with a mean value of 24.6 ± 2.5 cm s^{-1} over the entire depth range. Some bubbles entering the acoustic image at shallower water depths exhibited a slower rise velocity of 22.2 ± 2.4 cm s^{-1} and likely originated from adjacent emission sites. Measured rise velocities were too slow to be clean, uncoated bubbles. We therefore assumed that the bubbles were surfactant coated with a Gaussian-shaped size distribution peaking at an observed radius of 7500 ± 100 μm. If the flux derived from these measurements was assumed to be relatively constant over time, total methane issuing from only one of the ~20 active bubble vents at the pockmark site is estimated as ~9 kg yr^{-1}, similar to the flux from other reported marine CH_4 vent sites.

INTRODUCTION

Geologic marine methane (CH_4), a potent greenhouse gas, has sources in a variety of environments that include gas hydrate deposits, mud volcanoes, and natural gas seeps located on all continental margins (Judd, 2003; Reeburgh, 2007). Globally, marine seeps are suggested to contribute significantly to atmospheric methane inventories (Judd et al., 2002; Badr et al., 1991). Marine geologic CH_4 sources, including continental margin seeps, contribute an estimated 20–30 Tg yr^{-1} (1 Tg = 10^{12} g), with terrestrial microseepage and mud volcanoes contributing an additional 30–55 Tg yr^{-1} (Kvenvolden et al., 2001; Judd, 2004; Etiope et al., 2009) out of a total methane budget flux of 580 Tg yr^{-1} (Solomon et al., 2007). In some instances, methane seeps form shallow depressions in the seafloor known as pockmarks, which are proposed to result from the collapse of a void or a result of overpressurization of gas phase hydrocarbons within the sediment (Hovland and Judd, 1988; Leifer et al., 2006).

Methane seeps exhibit significant temporal variations in vent behavior that strongly influence the ability to make accurate flux estimates. Several previous studies have examined vent source behavior over intervals that spanned multiple years (Heeschen et al., 2005; Bradley et al., 2010), tidal periods (Boles et al., 2001; Tryon et al., 2002), and ocean swell time scales (Leifer and Boles, 2005). However, due to the difficulty in measuring bubble flux, few quantitative measurements of marine seep methane flux have been made. Video imaging has been used (Leifer and MacDonald, 2003; Sauter et al., 2006), but the technique is difficult to apply for long-term monitoring, particularly if the vent emission site is nonstationary. A variety of acoustic methods also has been used in previous studies (Hornafius et al., 1999; Heeschen et al., 2005; Nikolovska et al., 2008; Greinert et al., 2010).

In this study we used an upward-looking acoustic mooring anchored on the seafloor and analyzed the reflected returns to measure the rise velocity of methane bubbles emitted from a seepage site associated with a carbonate-lined pockmark. The rise velocities then were used to derive a bubble radius distribution, a critical factor in determining the fate of the seep gas flux into the water column and atmosphere. This approach also has several advantages, including relatively low cost and demonstrating the potential for long-term observations of gas phase emissions from source vents. We also present data showing the physical impact of the methane bubble plumes on the behavior of mesozooplankton scattering layers.

GEOLOGICAL AND HYDROLOGICAL SETTING

The Cascadia subduction zone extends from northern California (USA) to Vancouver Island (British Columbia, Canada), and is formed by the Juan de Fuca plate obliquely subducting beneath the North American plate at 42 mm yr^{-1} near the latitude of our study site. The margin complex is characterized by seaward-vergent imbricate thrust slices of accreted sediments that are separated by landward-dipping listric faults (McNeill et al., 1997). The Washington State (USA) continental margin is formed from a segment of this accretionary complex, and the near-surface sediment layers are composed largely of continentally derived turbidities and hemipelagic mud (Sternberg, 1986; Flueh et al., 1998).

The Washington continental margin occupies 250 km of the Cascadia subduction zone, from the Strait of Juan de Fuca to the mouth of the Columbia River, and is relatively narrow (40–60 km) compared to other North American continental margins. The shelf structure consists of sediments ranging from Pliocene to Miocene in age (Ritger et al., 1987); the shelf break occurs at ~175 m depth (Sternberg, 1986). Mud diapiric intrusions have been commonly imaged at several sites along the Cascadia margin, and are evidence of an active high pressure fluid system deep within the accretionary wedge (Silver, 1972; Fisher et al., 1999; Paull et al., 2008).

Methane emissions on the Washington margin are believed to be produced within the mélange and broken formations, which form much of the Cascadia accretionary complex in our study area

*Corresponding author: maries3@u.washington.edu.

Geosphere; December 2011; v. 7; no. 6; p. 1273–1283; doi: 10.1130/GES00648.1; 10 figures.

(McNeill et al., 1997). Records of prehistoric Pliocene methane vents have been described on the Washington coast, and there is a currently active terrestrial vent that produces thermogenically derived methane located 63 km east of our study site (Martin et al., 2007). Other similar vent sites located offshore along the Oregon Cascadia margin also have been noted to derive largely from thermogenic sources (Collier and Lilley, 2005; Torres et al., 2009). Methane carbon isotopic ratios from the Grays Harbor (Washington State, USA) pockmark have not been measured, but commercial drilling on the shelf near our site recovered long-chain hydrocarbon gases and oil traces, indicative of a thermogenic origin (Palmer and Lingley, 1989).

The physical oceanography of the Washington margin has been studied intensely (Hickey, 1979, 1997; Hickey and Banas, 2008). The area of the Washington shelf near Grays Canyon has systematic seasonal upwelling from mid-water depths in the summer and downwelling in the winter. It also is an area of high nutrient concentrations and high primary production, along with seasonal subthermocline hypoxic conditions present in most years (Hickey and Banas, 2008; Connolly et al., 2010).

METHODS

In this study we examined a pockmark recently discovered on the Washington continental margin near Grays Canyon. The study site is located near 46.886° N, 124.774° W (Fig. 1). A small Phantom remotely operated vehicle (ROV) photographed the seabed emission site and collected samples in the pockmark area in August 2008 and September 2009. The water column was characterized by CTD (conductivity, temperature, depth) casts in June 2007 and September 2009, along with analysis of Niskin bottle samples from a cruise on the R/V *Thomas G. Thompson* in June 2007.

Acoustic data were collected from 12 to 14 September 2009 using a 200 kHz acoustic water-column profiler (ASL Environmental Sciences, Victoria, Canada). The acoustic profiler had a vertical and upward orientation and was located in 150 m water depth. The deployment site was ~6 m from the nearest methane bubble stream at 46.885° N, 124.777° W, where the position is based on integrated ship-board sonar and ROV observations. This location was on the west-southwest side of the pockmark (Fig. 1), where ROV video confirmed multiple (>5) sources of individual bubble vents. The profiler location was determined at release and was based entirely on the global positioning system position of the surface ship, thus the actual seafloor mooring site position has some uncertainty.

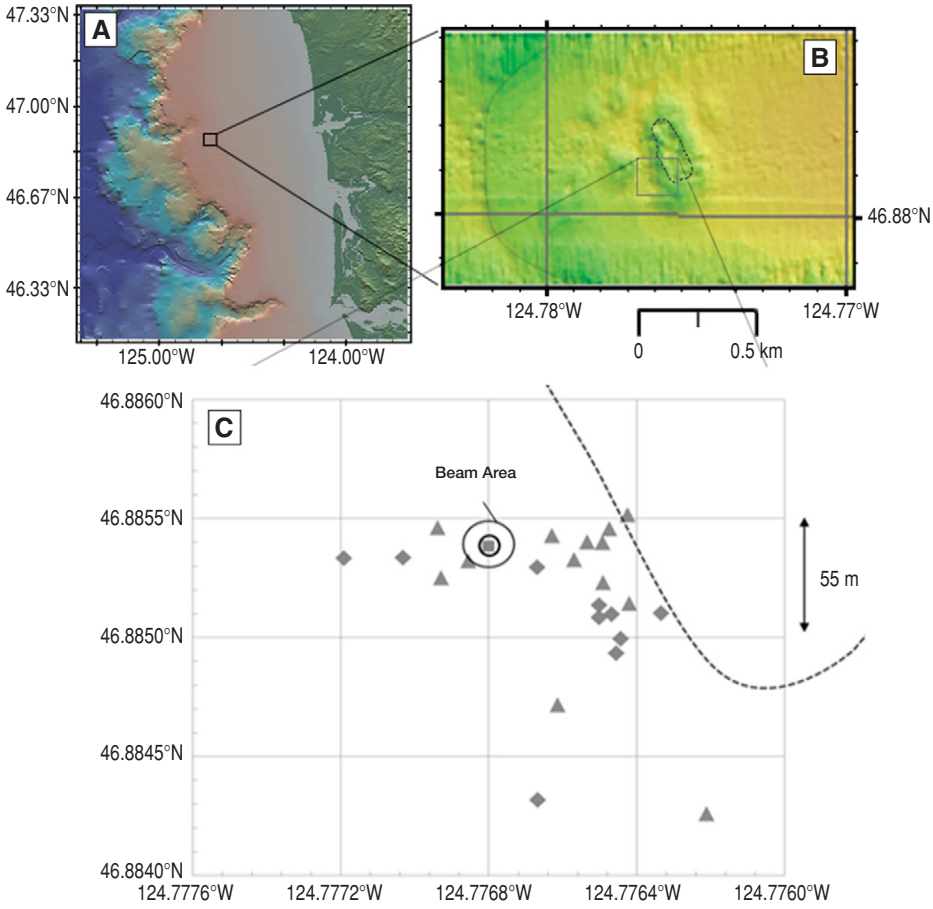

Figure 1. (A) Location of acoustic mooring at the pockmark site on the outer continental shelf offshore Grays Harbor (Washington State, USA). (B) Pockmark site is at a depth of ~150 m; nearby sinuous fault is outlined in gray. (C) Estimated distribution of active methane plumes on the southwest side of pockmark. Bubble stream locations were estimated based on remotely operated vehicle video (diamond) and ship-mounted sonar surveys (triangle). Circles around the profiler mooring location (square) represent the area of the acoustic beam at 50 m (small circle) and 110 m (large circle) above the seafloor. Dashed line corresponds to the edge of the pockmark crater. Note: there are ~20 locations where bubble streams were detected in this survey area, although some are possibly redundant due to navigation error.

The geometry of the acoustic profiler beam was specified by the manufacturer as 8° full width (≥3 dB; Fig. 2), resulting in an observation cone with a cross-section area of 0.32 m^2 at 140 m water depth, expanding to 137 m^2 at 50 m water depth. The integrated acoustic backscatter was binned in 0.91 m range bins. The profiler was mounted on a 5 m tall mooring, allowing observations to a distance of ~100 m, imaging water-column depths from 48 to 144 m. Thus, observations did not include either the upper photic zone or the immediate near-bottom layer.

Acoustic data were collected continuously at 1 Hz for ~33 h (117,625 s) (Fig. 3). For bubble size measurements, data were subsampled for 200 s periods at 15 min intervals to make the data set size manageable (total of 7.33 h of data). Within these discrete sampling periods, each visible bubble path was manually measured from the range-time profile to determine the rise velocity (in cm s^{-1}) using the program ImageJ (Rasband, 2010). Bubble rise velocities (Fig. 4) then were converted into two sets of equivalent spherical radii for two cases, (1) clean, surfactant-free bubbles and (2) surfactant-coated bubbles, based on rise velocity parameterizations (Leifer and Patro, 2002, their equations 14 and 15). For the case of clean bubbles, the rise velocity as a function of radius exhibits a maximum at the onset of volume oscillations (Fig. 4), and thus bubble radius as a function of rise velocity is not single valued (Leifer and Patro, 2002).

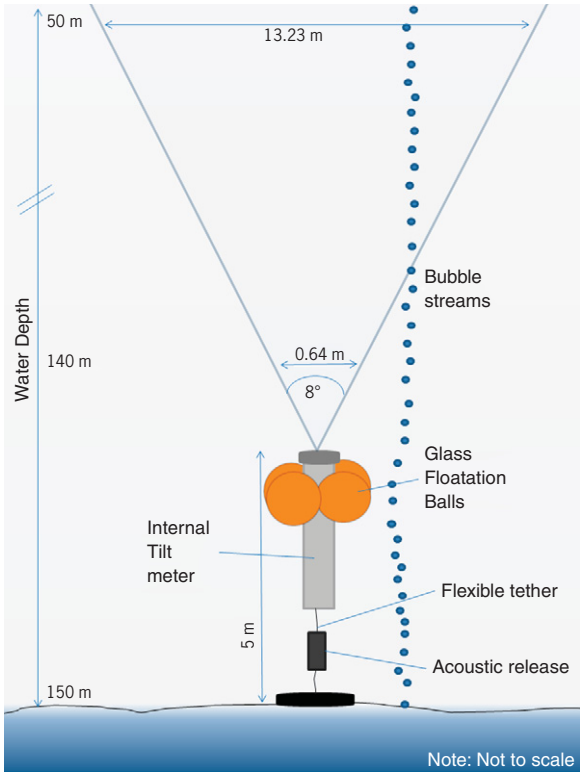

Figure 2. Diagram of the acoustic profiler-mooring configuration. Vertical dimensions are not to scale.

The bubble size distribution was derived by calculating a histogram for logarithmically spaced radius bins. Gaussian functions were fit to the size distribution with the curvefit toolbox in Matlab Version 9.0 (Mathworks, http://www.mathworks.com/index.html). Dirty and clean bubbles have different size distributions, allowing for the possibility of as many as three distinct potential radii for a single rise velocity measurement. Here, dirty and clean refer to the hydrodynamic effect of surfactants (Leifer and Patro, 2002), which are molecules with both hydrophilic and hydrophobic components. Although surfactants are ubiquitous in marine waters (Zutic et al., 1981), Patro et al. (2002) showed that larger bubbles in seawater behave as hydrodynamically clean in any case. This is because fluid motions from the rising gas compress surfactant films to the bubble's downstream hemisphere, where they have minimal effect on bubble hydrodynamics (Duineveld, 1995). The general case of whether bubbles emitted from seabed methane vents associated with bacterial mats are either dirty or clean has not been determined.

For a 200 kHz frequency sonar signal with a wavelength of 0.75 cm in seawater, the acoustic return intensity is highest for bubbles with approximately the same diameter length scale as the characteristic wavelength required for detecting zooplankton (Stanton et al., 1996; Greinert and Nutzel, 2004). Zooplankton scattering layers, commonly found at mid-water depths throughout the ocean, present additional backscatter targets with acoustic intensities similar to methane bubble streams. Biological and bubble acoustic reflectors were differentiated largely by their behavior, with uniformly ascending targets assumed to be gas bubbles, and stationary or slowly moving targets interpreted as fish and zooplankton. Biological acoustic returns are also identified by their quasi-horizontal distribution in the water column and characteristic diel vertical migration behavior (Thomson and Allen, 2000) (Fig. 5). This interpretation was confirmed by video images acquired during ROV dive deployment and recovery transits, as well as discrete-depth zooplankton tows made at the site during the cruise.

RESULTS

Study Site

The seabed expression of the main pockmark is oblong in shape, 240 m in length by 100 m in width (Fig. 1), and is within the mid-shelf mud deposit that covers much of the Washington shelf at this latitude (Nittrouer, 1978; Sternberg, 1986). Based on swath bathymetry data, the pockmark center contains a collapsed depression filled with chaotically oriented carbonate plates with only a few meters of relief. Other smaller mounds are located in the near vicinity of the main pockmark, within ~100 m of the central depression. A large sinuous fault is visible in swath bathymetry image located <1 km west of the main pockmark (Fig. 1). This fault vertically displaces the seafloor by 1–2 m and appears to be the seabed expression of one of the listric normal faults in the area described by McNeill et al. (1997).

In both 2008 and 2009, video from multiple ROV dives conducted over several days showed multiple bubble streams issuing from beneath displaced carbonate plates that were located inside an area of several square meters near the center of the pockmark. Visual observations over short time periods suggested that emissions were at a relatively steady rate of one bubble every several seconds from each discrete vent source. Several vent sources were often visible simultaneously in a single ROV video image. Bubble radii from the ROV video subjectively appeared to be on centimeter size scale, based on bubble eccentricity, which changed substantially over short time intervals. However, the size scale for the video images was uncalibrated and thus highly imprecise. Based on ROV video and ship-mounted sonar survey (Fig. 1), it was estimated that the emission site nearest the mooring was located directly within the lowermost edge of the acoustic detection cone of the profiler, at a horizontal distance of <6.8 m. Other active bubble emission sites observed by ROV were located within 10–20 m of the mooring site.

Water Properties

In 2007, a CTD profile near the bubble plume showed a thick bottom boundary layer with a remarkably uniform bottom layer of salinity and temperature extending from 100 to 150 m depths to within 5 m of the seafloor. This uniform bottom boundary layer was also observed to be present in June 2009, but was thinner and less uniform. Both the June 2007 and September 2009 CTD data showed a temperature change of ~0.5 °C that peaked at a depth of ~80 m (Fig. 6A). Methane concentrations were measured directly over the pockmark plume from Niskin bottle samples during the 2007 cruise (Fig. 6C). The maximum methane concentration observed within the water column was 441 nM from a Niskin bottle taken 5 m directly above the pockmark, with methane concentrations rapidly decreasing toward the surface. Elevated methane concentrations of 13–16 nM were measured at the sea surface (~1 m water depth), compared to the ambient CH_4 concentration of ~1 nM off the Cascadia margin (Collier and Lilley, 2005). This strongly suggests that the methane bubbles, which were visually observed rising to

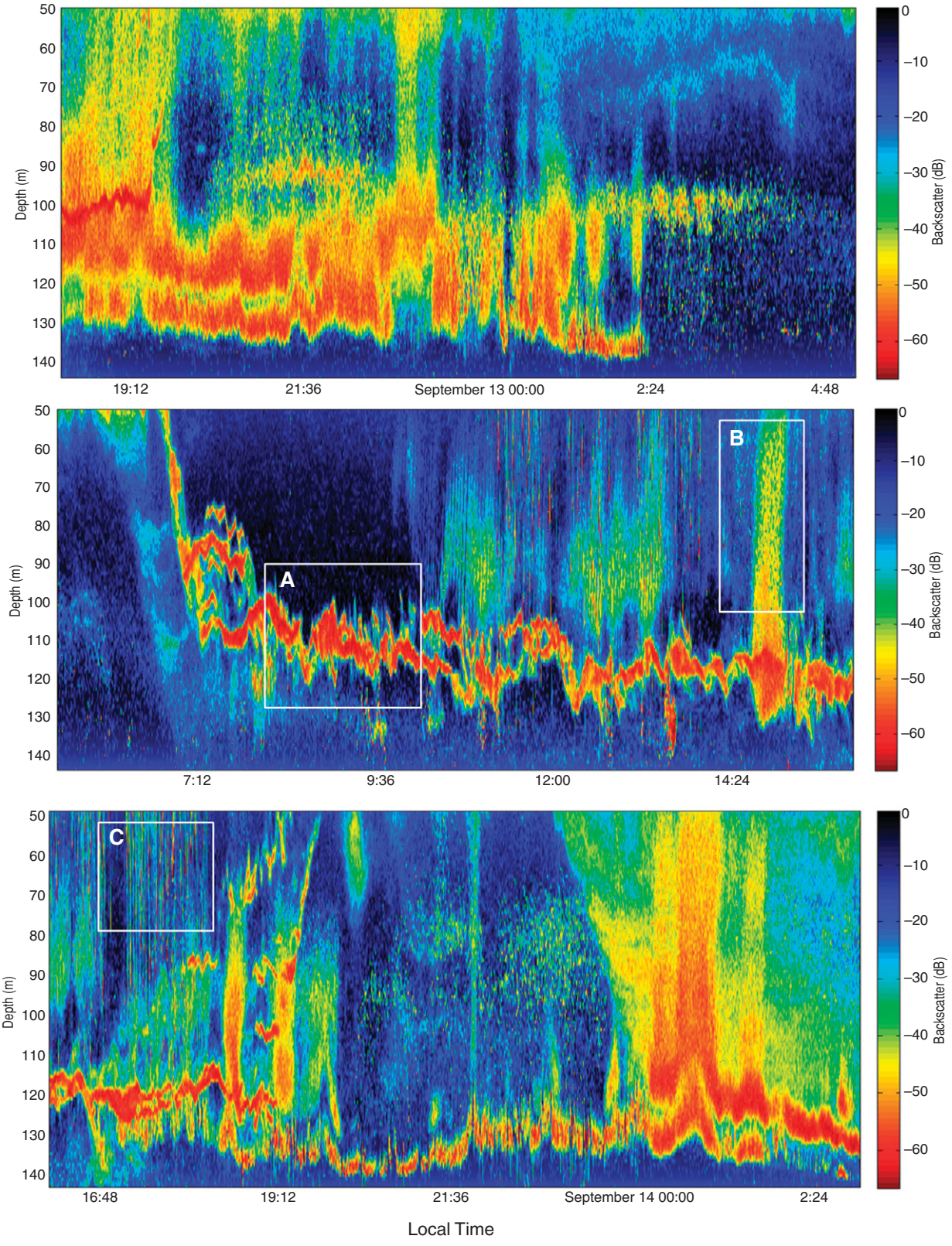

Figure 3. Full data set from acoustic profiler, 18:30 Local Time (LT) 12 September to 03:00 LT on 14 September. The false image with bright colors corresponds to strong acoustic returns. Time series begins on the left (top panel) and ends in the right (bottom panel). Rising bubble streams (outline A) are vertical lines at this compressed scale, while zooplankton scattering layers (outline B) are irregular semihorizontal bands. Note diurnal descent or ascent of zooplankton, presumed euphausids, at 06:45 and 19:00 LT 13 September. There was a hiatus in bubble emissions from 02:30–09:30 LT 13 September. High-intensity noise (outline C) is an artifact from the ship-mounted 200 kHz sonar.

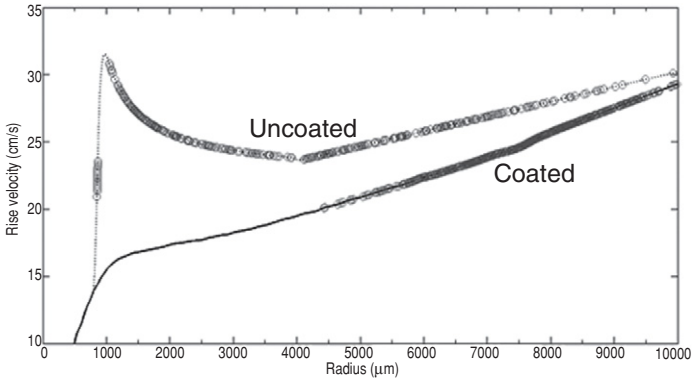

Figure 4. Plot of equations used for the rise velocity parameterization in the derivation of equivalent bubble radius (based on relationships in Leifer and Patro, 2002). Solid line shows single-valued increase in rise velocity and bubble radius for surfactant-coated bubbles, the assumption used in this study. Dashed line shows multivalued relationship for hydrodynamically uncontaminated bubbles. Gray circles are the values used in the rise velocity radius conversion.

the sea surface, still contained significant methane. Gas chromatographic measurements (SRI Model 8610c, http://www.srigc.com/) revealed that atmospheric methane concentrations over the pockmark location were 0.5 ppm above the ambient levels measured distant from the vent sites. Anomalously high dissolved silica concentrations derived from sediment pore waters were observed within the near-bottom layer, suggesting vertical transport in the water column by the methane bubbles (Fig. 6C). Silica concentrations remain elevated within the bottom waters to a depth of ~100 m, corresponding to the bottom uniformly mixed layer.

Biology and Bubbles

Fauna documented in the area of the vents by ROV video, sonar data, and plankton net tows included dense schools of rock fish and rattail fish, large aggregations of euphausiids (krill), chaetognaths, and other zooplankton. Benthic geological structures (carbonate plates and mounds) directly adjacent to vents were colonized by sponges and white bacterial mats, indicative of significant temporal persistence of the methane emissions.

The 200 kHz sonar frequency is designed to detect zooplankton and other biological targets, which were present at our site in nearly contiguous, horizontal scattering layers at 120–140 m depth, located ~20–30 m above bottom in the areas near the methane plumes. Based on ROV dives and plankton net tows in 2009, these scattering layers were identified as dense krill and chaetognath aggregations. During the period of the mooring deployment, a portion of the biological scattering layers ascended and descended on a diurnal basis, as previously reported for krill (Thomson and Allen, 2000). During periods when the acoustic backscatter indicated that the upward bubble flow throughout the water column was unusually intense, the sonar images showed a corresponding 5–10 m uplift and general diffusion of the normally well-defined biological scattering layers within the water column (Fig. 5). This uplifting of the zooplankton layer was only observed during the more intense bubbles stream emissions, but was a recurring feature also observed by the ship-mounted sonar on multiple visits to the site. The gas-seawater density difference of the bubble streams provided the seep bubbles with a very high intensity backscatter signal compared to individual zooplankton in the scattering layers. However, the very dense zooplankton concentrations occasionally completely obscured the gas bubbles as they rose vertically through a horizontal biological scattering layer.

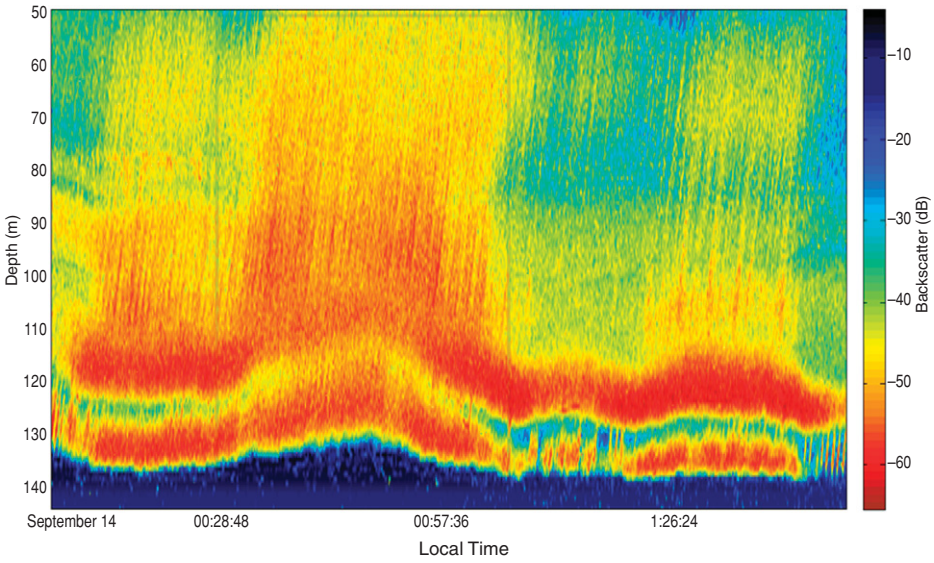

Figure 5. Example from the mooring profiler of a period of high-intensity bubble emissions from the pockmark site that appears to affect the depth of zooplankton scattering layers. Image suggests that some zooplankton temporarily were entrained in the rising bubble plume and redistributed higher in the water column.

Bubble Rise Velocities and Size Distribution

The sonar data showed high variability in methane bubble emission rate over the entire observation period. Continuous methane bubble emissions were observed from 1840 Local Time (LT) 12 September to 0225 LT 13 September, and from 1000 LT to slightly after 2400 LT on 14 September (Fig. 3). An ~7 h hiatus was observed in bubble emission from 0225 LT 13 September, although abundant biological scattering targets indicated normal profiler function. Note in Figure 3 that the acoustic noised recorded at ~1100–1300 LT 13 September was due to interference from the shipboard 200 kHz sonar during simultaneous surveys in the mooring area.

For analysis, we classified bubble behavior in the sonar data into three general categories. The first category consisted of bubbles that rose continuously through the entire profiler depth range (Fig. 7A). Although the seafloor profiler's truncated range prevented sonar confirmation

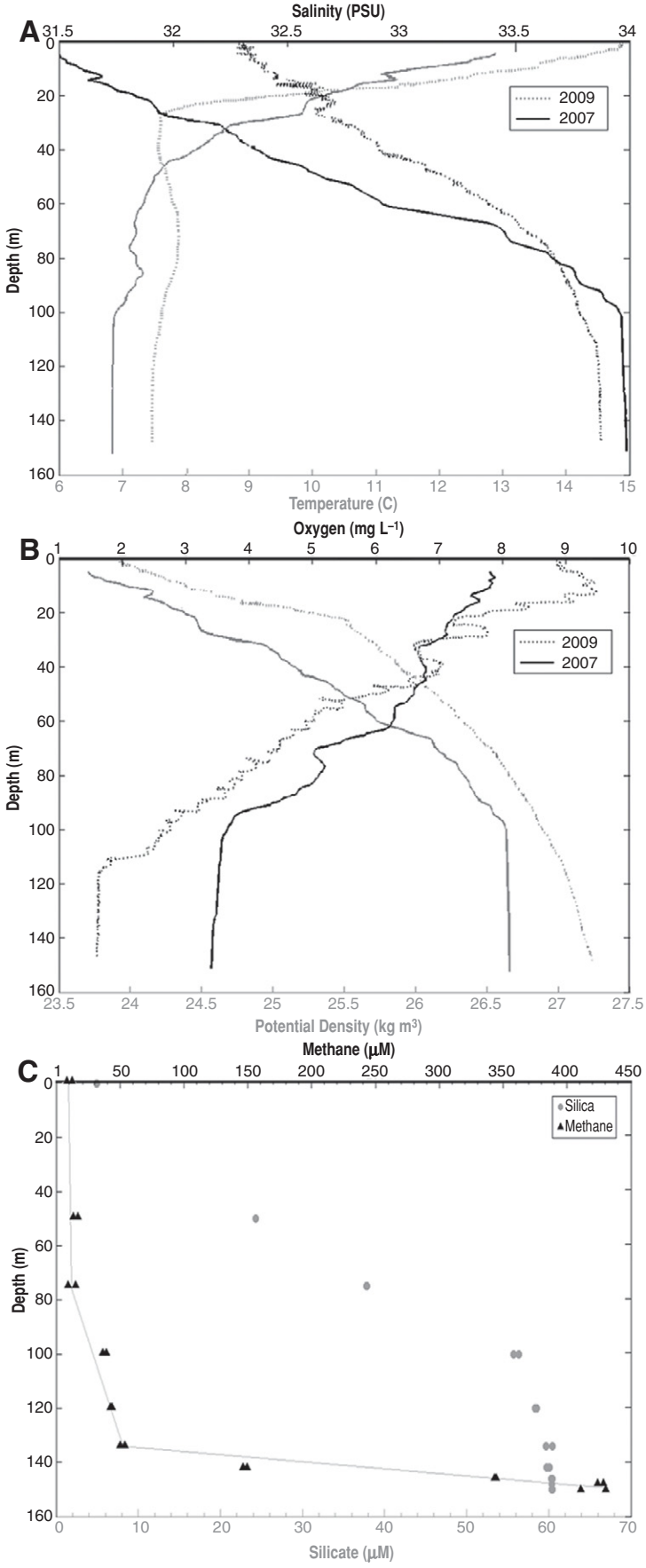

Figure 6. Water-column properties measured with two CTD (conductivity, temperature, depth) casts over the pockmark site. (A) Showing strong seasonality in temperature (gray) and salinity (black; PSU—practical saline units). (B) Density (gray) with oxygen (black). Data collected in September 2009 are dotted lines and June 2007 data are continuous lines. Note a local increase in the temperature peak at 80 m in 2007 and at 70 m in 2009 in A and a thick bottom boundary that varies in thickness in both profiles. (C) Methane (black triangles) and dissolved silica (gray circles) concentrations over the pockmark site were taken in 2007 using Niskin bottle casts in the bubble stream over the pockmark site. Note that both methane and silica concentrations show changes at the top of the bottom boundary layer.

of bubble surfacing, the shipboard downward-looking acoustic profiler imaged bubble streams reaching the near-surface water column (Fig. 8). Shipboard observers occasionally observed a few bubbles reaching the sea surface, although sea state generally prevented useful surface visual observation. The second category of bubble behavior consisted of bubbles with high backscatter intensity that entered the profiler's view 3–5 m above the profiler transducer head. Bubble streams in this second category then disappeared from view at the approximate depth of the deep biological scattering layer, between 135 and 125 m below the surface (Fig. 7B). The third category of bubble stream behavior included bubbles that first appeared in the field of view at mid-water depths, at the upper end of the profiler's range (Fig. 7C). These mid-water bubbles appeared with an ~2 min episodicity.

Bubbles that traversed the profiler view over vertical distances from 70 to 30 m in depth (category 1) permitted a more accurate estimation of rise velocity (slope of the time versus depth) compared to bubbles, which only intersected the lower half of the profiler's view (category 2). Typical mid-water-column bubble tracks were 10–60 m long in vertical distance. We analyzed 1346 individual bubbles with a mean rise velocity of 24.6 ± 2.5 cm s^{-1}. Of the 1346 measured bubble tracks, 312 were bottom-water transit (category 2) and 834 were full-column transit bubbles (category 1) with mean rise velocities of 25.5 ± 2.7 and 24.8 ± 2.1 cm s^{-1}, respectively. There were 200 measured bubble tracks that appeared only higher in the water column (category 3), and these had a slower mean rise velocity of 22.2 ± 2.4 cm s^{-1}. The range-time slope uncertainty was estimated based on deviations from linear in the pixelated lines and was ±0.8°, equivalent to a rise velocity uncertainty of ±0.008 cm s^{-1}.

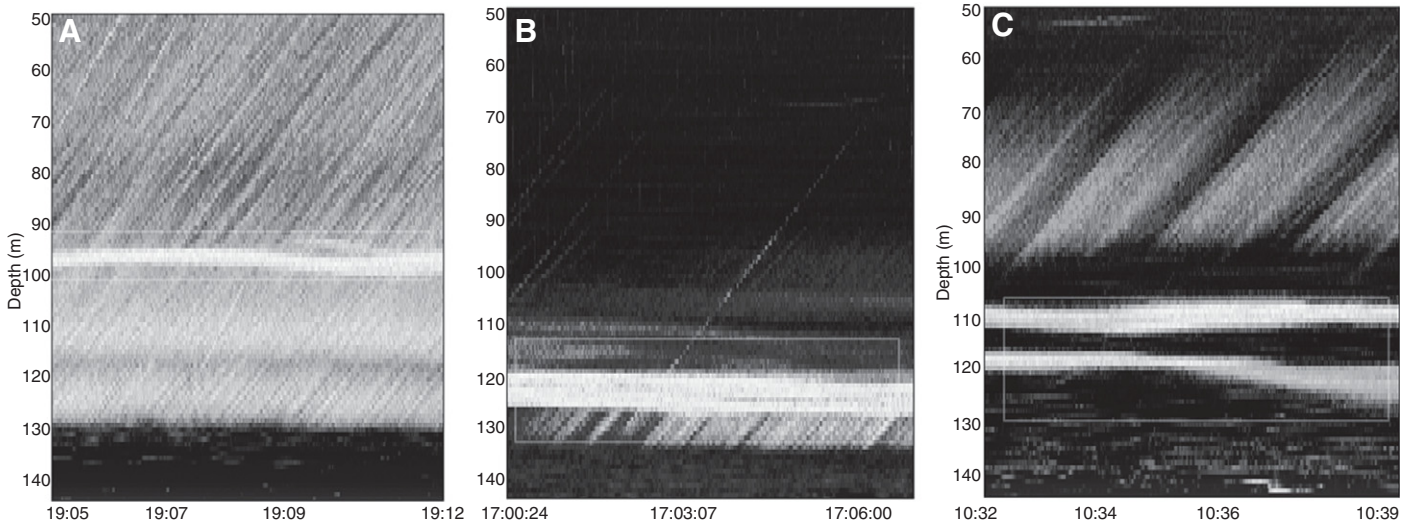

Figure 7. Clockwise, starting with top left: examples of bubbles streams. (A) Rising through full water column (19:05 Local Time, LT, 12 September). (B) Constrained to the near-bottom layer (17:00:24 LT 13 September) (C) Only present in the upper water column (10:32 LT 13 September). Biological scattering layer is outlined in a gray box.

Assuming that the observed bubbles were surfactant coated, the calculated size distribution (Fig. 9) implies that bubbles detected both only near the seafloor (category 2) and those present throughout the water column (category 1) had size distributions with very similar shapes. Bubbles that transited the entire water column had a mean radius of 7500 ± 1000 µm and their distribution was well described (R^2 = 0.953) by a Gaussian function with maximum at 7800 µm and half-width of 1400 µm. Bubbles occurring only near the seafloor had a mean radius of 7700 ± 1000 µm and were well fit by a Gaussian distribution (R^2 = 0.907) with a peak at 7800 µm and half-width of 1500 µm. For the clean bubble assumption, the bubble size distributions for the full (to 50 m depth) and bottom water-column profiler range (categories 1 and 2) had possible mean radii of 2200 ± 800 µm (±900 µm for bottom water column) and 6000 ± 1300 µm (Fig. 9). Radii solution distributions for the clean bubbles were skewed toward smaller radii for both bottom and full water-column bubbles and were not Gaussian in shape, unlike most typical seep vent bubble size distributions (Leifer, 2010).

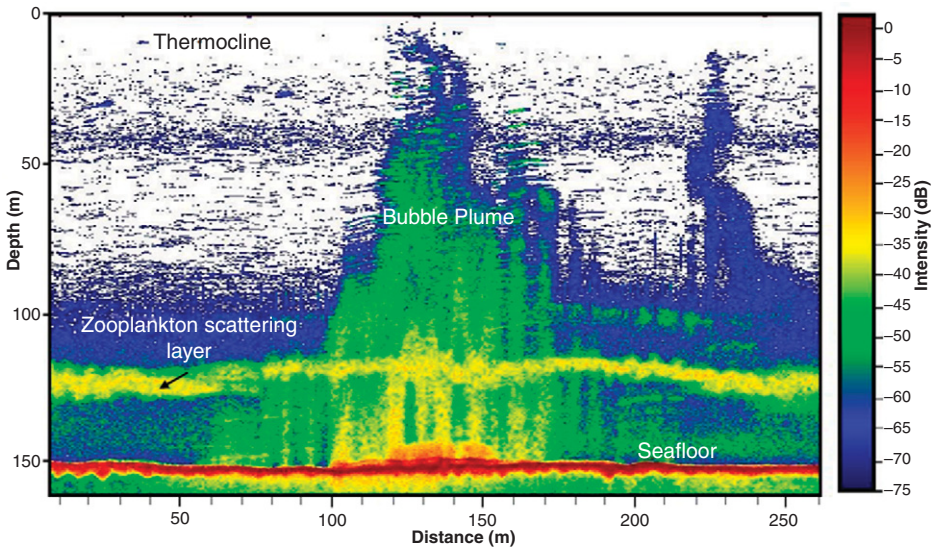

Figure 8. Downward-looking sonar image over the pockmark of the methane plume. Image of the pockmark bubble plume is from the ship-mounted 200 kHz sonar.

DISCUSSION

ROV video shows large areas of carbonate plates near the bubble emission site within the pockmark area on the Washington margin that are common to many methane seep locations at other sites (Carson et al., 1994; Suess et al., 2001; Hein et al., 2006; Paull et al., 2008). These plates provide evidence of substantial post-formation collapse of complex biogenic structures associated with the methane gas emissions (Hovland and Judd, 1988; Johnson et al., 2002). Based on the spatial distribution of observed gas emission sites near the mooring, there appeared to be at least two nearby clusters of multiple bubble streams, located just east and west of the profiler (Fig. 1), where bubbles could have been advected into the acoustic detection zone by bottom currents. During several observation intervals, the acoustic backscatter signal from bubbles faded in intensity, vanished, and then later reappeared within the profiler's view (Fig. 3). This intermittent behavior could be the result of changes in the source emissions, bottom currents horizontally transporting bubbles in and out of the profiler beam, or periodic strong bottom currents deflecting the orientation of the acoustic profiler mooring from vertical.

The bubbles observed only in the near-bottom field of view (category 2) had stronger acoustic backscatter intensity than full water-column bubbles (category 1), but did not exhibit a corresponding difference in rise velocity (Fig. 7). These bubbles may have disappeared from the field of view due to dissolution within the water column; this would occur more rapidly

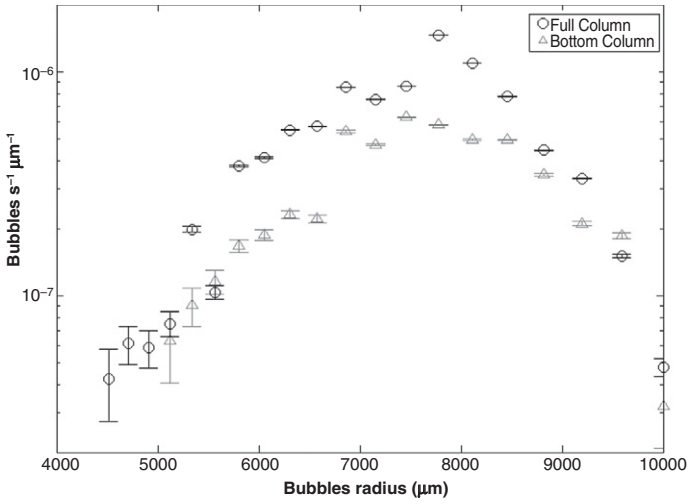

Figure 9. Bubble emission size distribution for surfactant-coated bubbles from pockmark bubble stream. Black circles are data from bubble streams that transited the full water column. Gray triangles are bubbles only observed in near-bottom field of profiler. Radius histogram bins are logarithmically spaced and flux has units of number of bubbles/µm/s. Flux uncertainty is $1/(n^{1/2})$ normalized to bin width, where n is the number of bubbles per histogram bin.

for smaller bubbles that lacked significant surfactant coating (Leifer and Patro, 2002). Horizontal transport of the bubble stream out of the acoustic beam by bottom current advection is also possible, although the 8° acoustic beam width widens significantly with height above the seafloor. The comparatively slower rise velocity of mid-water-column bubbles compared to the near-bottom and full water-column bubble categories suggests deceleration, and is consistent with bubble shrinkage due to gas evasion (Fig. 4). Bubbles with slower rise velocities are more susceptible to horizontal transport by currents and subsequent advection into the sonar detection cone at mid-water depths from a nearby source vent.

Biology and Bubbles

Vertical transport of entrained bottom water by the rising bubble stream (Leifer et al., 2009) is the most plausible cause of the apparent upward displacement of the biological scattering layer observed during intense bubble emission. Since the sonar beam only recorded the scattering layer along a single vertical profile, it is not clear whether individual zooplankton from the disturbed layer remained redistributed throughout the water column or descended to their original depth following the interaction with the high-intensity rising bubble stream. Uplifting of a zooplankton layer was only observed with the more intense bubbles stream emissions, which should exhibit stronger entrained upwelling flows, a process that has been previously reported for engineered bubble plumes (Grimaldo et al., 2011). This suggests that the weaker upwelling flows of the less intense plumes and individual bubbles created insufficient advection to displace the biological scattering layer, or the zooplankton may have actively opposed the weaker entrained flow by swimming.

Although poorly understood, the development of horizontal zooplankton layers in seawater is thought to be controlled by both physical and behavioral processes. Biological scattering layers have been related to sharp vertical density gradients and regions of low advection (Cheriton et al., 2007; Sevadjian et al., 2010). Horizontal layering also may arise behaviorally, when organisms reach conditions such as preferred light intensities, buoyancy layers, prey aggregations, conspecifics for mating and defense, or reach minimum tolerable temperatures or low oxygen levels. For euphausiids, diel vertical migration is traditionally explained by the need to avoid visual predators during daytime and return to feed near the sea surface during night, with the daytime depth potentially set by either light levels (Kaartvedt et al., 1996) or temperature (Sameoto, 1982). Therefore, an alternate mechanism for the changes in scattering layer depth during periods of vigorous bubble streams observed in our study could be that bubble-induced water-column changes in turbidity, light levels, or temperature may have resulted in a behavioral shift in distributions. We consider this hypothesis less likely than the more direct mechanism of entrainment of the zooplankton in upwelling water plumes driven by the buoyancy of the bubble streams, but unfortunately we do not have the data to test either hypothesis.

Bubble Size Distribution and Total Flux

We cannot definitively prove that the bubbles observed in this experiment were coated with surfactants from bacterial mats at vent orifices. However, the observation that most of the bubble streams ascended with a relatively constant velocity and survived the full 150 m transit through the water column argues strongly that most of the bubbles emitted from the pockmark site were hydrodynamically dirty (Leifer and MacDonald, 2003). Specifically in our study, the implication is that the bubbles are coated with biofilm surfactants from the observed high biological productivity within the methane vent area.

For the category 1 and 2 surfactant-coated bubbles, the near Gaussian shape of the bubble size distribution, when estimated assuming surfactant coating and relatively constant rise velocity, suggests negligible change in bubble size with depth, consistent with the larger bubbles predicted for surfactant coasting than for the clean bubble assumption. Although plausible, there is some circularity in this argument. In Leifer (2010) it was reported that methane bubble plumes without significant turbulence were well described by a Gaussian function. The slight bimodal distribution in our bubble size distributions (Fig. 9) provides evidence for two different bubble populations. Furthermore, the bubble size distribution exhibits a peak radius at very large bubbles, approaching the size where bubble breakup occurs (Clift et al., 1978). Strong surfactant contamination would stabilize these bubbles against breakup by lowering their rise speed (i.e., decreasing the Reynolds number). Larger bubbles behave as hydrodynamically clean even in heavily contaminated waters where heavy surfactant contamination also is likely (Patro et al., 2002).

The similarity found between the size distribution of clean category 1 and 2 bubbles suggests that significant bubble dissolution did not occur during transit through the water column (Fig. 10). Clean bubbles exhibit rapid transfer of gas to the liquid phase, producing a rapid size change with time and a short bubble lifetime (Leifer and Patro, 2002). This strongly supports the conclusion that the majority of the bubbles observed in the sonar images at this

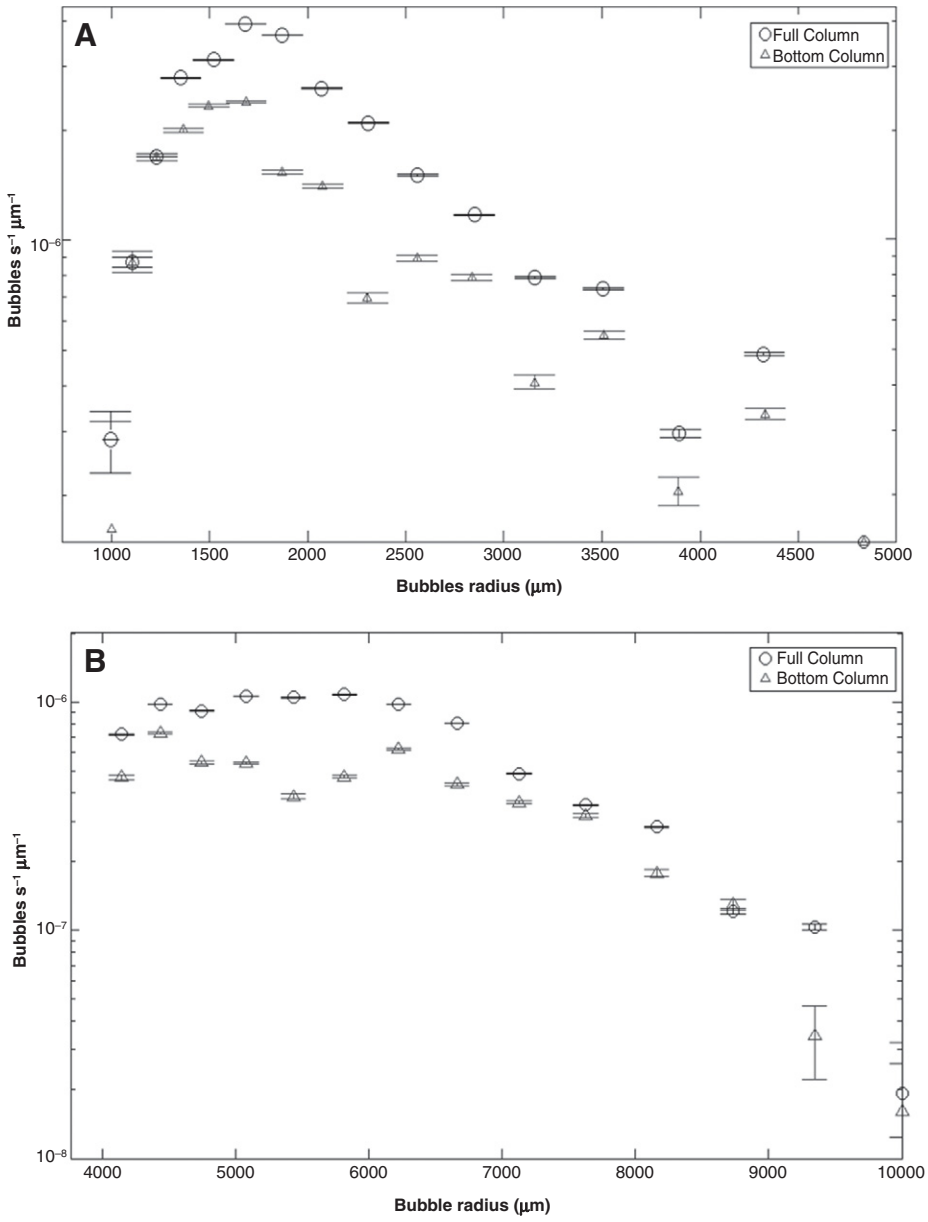

Figure 10. Bubble emission size distribution for hydrodynamically clean bubbles. (A) For small-radius solutions from pockmark bubble stream. (B) For large-radius solutions from pockmark bubble stream. Black circles are data from bubble streams that transited the full water column. Gray triangles are bubbles only observed in near-bottom field of profiler.

site are surfactant coated. The magnitude of the surfactant impact on bubble velocity depends on the surfactant characteristics (Leifer and Patro, 2002). Surfactant contamination such as from liquid hydrocarbons both limits exchange between bubbles and seawater and reduces the bubble rise velocity (Leifer and MacDonald, 2003), extending the vertical distance that a bubble can transit after seafloor emission (Leifer and Patro, 2002). Surfactants such as polymucosaccharides derived from biological sources can produce similar effects (Leifer and Patro, 2002). A likely source of bubble contamination is from biofilms derived from sediment microbial methanotrophs, particularly those observed within the biologically rich methane seep areas of our emission sites. Oil-coated bubbles are unlikely at this site, given the absence of visible oil sheens at the sea surface during the three cruises of this study, although traces of oil within the sediment subsurface have been found in nearby areas of the Washington margin (Palmer and Lingley, 1989).

Water-column properties such as temperature and currents can play a major role in the vertical methane distribution from seep bubbles and bubble plumes. As an example, an inflection in the vertical density profile appears to be correlated with the temperature profile and is consistent with a plume-driven mid-water intrusion at 30–40 m depth observed in 2009 (Fig. 6B). The water-column profiles also show the corresponding significant mid-water anomaly in salinity at 20–35 m in 2009 (Fig. 6A), an anomaly expected of bubble-plume driven intrusions (Lemckert and Imberger, 1993). On at least a local scale, methane bubble plume transport processes could affect levels of dissolved oxygen by redistributing near-bottom water throughout the water column. Due to the wide vertical spacing of the Niskin bottle water samples, it was not possible to determine if the variations in dissolved silica and temperature vertical profiles are well correlated; however, the general similarity in profile shape and depth suggests a common mechanism.

Methane Flux

Quantitative determination of the methane flux from coastal marine seeps is challenging due to the large uncertainty in bubble sizes within a rising stream, temporal variability within the seafloor emission source, unresolved bubble dissolution, dynamic gas phase composition, and spatial variability of the seabed emission locations. However, even order-of-magnitude estimates are valuable to gain a better understanding of the contribution of individual seeps to marine biological and geochemical processes.

For the surfactant-coasted bubble emission size distribution, the estimated methane emission from the area directly adjacent the acoustic profiler mooring was 0.4 cm^3 CH_4 s^{-1} or 1.2×10^{-3} g CH_4 s^{-1}. This estimate assumes a 95% methane composition, which is based on measured gas composition from similar seeps on the Oregon continental margin with compositions that are 93%–98% thermogenic methane (Collier and Lilley, 2005). Extrapolation to an annual flux yields an emission of ~9 kg CH_4 yr^{-1} for the single bubble stream within the profiler view. This value is comparable to methane flux rates from individual bubble streams from vents at other sites, including off the Kattegat coast, Denmark, and in the North Sea (Judd, 2004). If the same calculations are applied to the hydrodynamically clean full water-column bubble emission distribution instead of the surfactant-coated model, the resulting fluxes from our study site would be ~3 kg CH_4 yr^{-1} and ~0.2 kg CH_4 yr^{-1} for large and small bubbles, respectively.

During periods when the seafloor bubble emissions were very high (Fig. 7A), the resulting acoustic backscatter saturated the data, increasing the difficulty in distinguishing individual bubble tracks. To compensate for this effect, the bubble size distribution was calculated only for a data subset with clear bubble tracks (Fig. 7A). Even with this correction, the total bubbles flux during these intense emission periods was likely undercounted, possibly by a factor between 2.5 and 5. For example, bubbles were visually observed during ROV dives to emanate at rates of 1–0.5 bubble s^{-1}, while acoustic bubble observations suggested a maximum emission rate of 0.19 bubbles s^{-1}, (over ~25% of the processed 7.33 h of data). Thus, our estimate represents a lower bound for this Washington pockmark site, with the actual annual methane flux from the study site likely being considerably higher, perhaps by a factor of 5–10 times higher. The acoustic sonar's limited observation cone and existence of other bubble emission sites observed using shipboard techniques (Fig. 1) suggest that the measured flux is only a small fraction of the total methane emissions from the pockmark site.

Fate of the Methane

A size-dependent fraction of the gas phase methane was transported directly to the atmosphere, with the remainder dissolving into the water column. Due to the shallow depth of these seeps, the dissolved methane within the water column likely transfers into the atmosphere over time faster than it is consumed by microbial degradation, although some fraction is microbially oxidized (Rehder et al., 2009). Further, some of the methane lost from the seep bubbles to the surrounding fluid is transported to the near surface by the upwelling flow of the bubble plume (Leifer et al., 2009). Where the bubbles and associated entrained bottom water rise as a plume through a change in density stratification, bottom seawater detrains into horizontal intrusions within the water column (Asaeda and Imberger, 1993). If these intrusions into mid-water eventually sink after loss of bubble buoyancy (because they include colder, denser, and more saline water), they induce mixing, which alters the water-column stratification over an area larger than the emission site, a process commonly used in terrestrial reservoir destratification (Schladow, 1993). This entrainment and intrusion process could explain some observed depth profiles of salinity, temperature, dissolved silica (a tracer of sediment pore fluids), and oxygen in the deep water column at the emission site. Specifically, the observed temperature inflection in the CTD profiles could reflect bubble plume–driven entrainment, which can elevate dense (cold, saline) water from near the seafloor to mid-water depths (Asaeda and Imberger, 1993; McGinnis et al., 2006; Leifer et al., 2009). However, absent wider geographical sampling to demonstrate the extent of the water-column anomalies, it also is possible that the observed nonuniform profiles result from regional physical oceanographic (i.e., non–bubble plume) processes.

CONCLUSIONS

A seafloor mooring with an upward-oriented 200 kHz acoustic profiler was used to monitor the behavior of a highly variable bubble plume over an actively venting methane seep at 150 m depth on the continental margin near Grays Canyon. Methane bubbles observed in near-bottom waters at ~130–140 m depths that had transited over the full 100 m profiler range had a mean vertical velocity of 24.6 ± 2.5 cm s^{-1}. These bubbles likely were surfactant contaminated, based on emission size distribution and the lack of change in rise velocity during their water-column transit. The bubble size distribution for the contaminated bubble assumption was well fit by a Gaussian function. Moreover, a significant fraction of the methane bubbles reached the sea surface, based on both acoustic and visual observations. Estimating the CH_4 flux and extrapolating to an annual basis suggests 9 kg CH_4 yr^{-1} for this single bubble stream source, and likely represents only a small fraction of the total site emissions.

The present experiment demonstrates that a bottom-mounted acoustic profiler mooring is a viable method for measuring both the long-term variability of seafloor methane emissions, and the potential interaction of these emissions with zooplankton scattering layers. Future improvements, such as the addition of a current meter to the mooring, would have aided the interpretation, particularly given the importance of bottom currents on bubble advection either into or out of the sonar measurement volume, although care is needed to prevent acoustic interference.

Sonar data showed that the rising bubble plumes apparently had a direct physical impact on the spatial distribution of zooplankton scattering layers near the emission site. In several instances, high bubble flux from the emission sites appeared able to at least temporarily redistribute the zooplankton scattering layers throughout the water column. These plankton scattering layers could potentially be targeted by predators, such as rock fish, that seek and exploit aggregations to increase their foraging efficiency. Displacement of the layer likely affects those processes, altering trophic interactions and carbon cycling. The full implications of the interactions between zooplankton and methane bubble streams remain unclear and represent fertile ground for future studies.

ACKNOWLEDGMENTS

We thank Tor Bjorklund and Tim McGinnis for assistance with the acoustic measurements and Dan Culling for assistance with the cruise and for the gas chromatography measurements. We also thank Mark Holmes and the crews of the RV *Thomas G. Thompson* and the *Kvichak Defender IV*. The map in Figure 1 was modified from images derived using the Lamont-Doherty Earth Observatory Marine Geoscience Data System application GeoMapApp software (http://www.geomapapp.org/). This study was funded in part by a grant from the Washington Sea Grant Program, University of Washington, pursuant to National Oceanic and Atmospheric Administration Award NA07OAR4170007, Project R/NP-6. An undergraduate research assistantship to Salmi was supported by the Washington Sea Grant Program. The views expressed herein are those of the authors and do not necessarily reflect the views of the National Oceanic and Atmospheric Administration or any of its subagencies, or the University of California, Santa Barbara. Additional support for this work was from National Science Foundation grant NSFOCE-0902626 and from the University of Washington College of Ocean and Fisheries Sciences.

REFERENCES CITED

Asaeda, T., and Imberger, J.T., 1993, Structure of bubble plumes in linearly stratified environments: Journal of Fluid Mechanics, v. 249, p. 35–57, doi: 10.1017/S0022112093001065.

Badr, O., Probert, S.D., and Ocallaghan, P.W., 1991, Atmospheric methane: Its contribution to global warming: Applied Energy, v. 40, p. 273–313, doi: 10.1016/0306-2619(91)90021-O.

Boles, J.R., Clark, J.F., Leifer, I., and Washburn, L., 2001, Temporal variation in natural methane seep rate due to tides, Coal Oil Point area, California: Journal of Geophysical Research, v. 106, no. C11, p. 27077–27086, doi: 10.1029/2000JC000774.

Bradley, E., Leifer, I., and Roberts, D., 2010, Long-term monitoring of a marine geologic hydrocarbon source by a coastal air pollution station in southern California: Atmospheric Environment, v. 44, p. 4973–4981, doi: 10.1016/j.atmosenv.2010.08.010.

Carson, B., Seke, E., Paskevich, V., and Holmes, M.L., 1994, Fluid expulsion site on the Cascadia accretionary prism: Mapping diagenetic deposits with processed GLORIA imagery: Journal of Geophysical Research, v. 99, no. B6, p. 11959–11969, doi: 10.1029/94JB00120.

Cheriton, O.M., McManus, M.A., Holliday, D.V., Greenlaw, C.F., Donaghay, P.L., and Cowles, T.J., 2007, Effects of mesoscale physical processes on thin plankton layers at four sites along the west coast of the U.S.: Estuaries and Coasts, v. 30, p. 575–590, doi: 10.1007/BF02841955.

Clift, R., Grace, J.R., and Weber, M.E., 1978, Bubbles, drops, and particles: London, Academic Press, 380 p.

Collier, R.W., and Lilley, M.D., 2005, Composition of methane seeps on the Cascadia continental margin: Geophysical Research Letters, v. 32, LO6609, doi: 10.1029/2004GL022050.

Connolly, T.P., Hickey, B.M., Geier, S.L., and Cochlan, W.P., 2010, Processes influencing seasonal hypoxia in the northern California Current system: Journal of Geophysical Research, v. 115, C03021, doi: 10.1029/2009JC005283.

Duineveld, P.C., 1995, The rise velocity and shape of bubbles in pure water at high Reynolds number: Journal of Fluid Mechanics, v. 292, p. 325–332, doi: 10.1017/S0022112095001546.

Etiope, G., Feyzullayev, A., and Baciu, C.L., 2009, Terrestrial methane seeps and mud volcanoes: A global perspective of gas origin: Marine and Petroleum Geology, v. 26, p. 333–344, doi: 10.1016/j.marpetgeo.2008.03.001.

Fisher, M.A., and 19 others, 1999, Seismic survey probes urban earthquake hazards in Pacific Northwest: Eos (Transactions, American Geophysical Union), v. 80, no. 2, p. 13, doi: 10.1029/99EO00011.

Flueh, E.R., Fisher, M.A., Bialas, J., Jonathan, R., Klaeschen, D., Kukowski, N., Parsons, T., Scholl, D.W., ten Brink, U., Trehu, A.M., and Vidal, N., 1998, New seismic images of the Cascadia subduction zone from cruise SO108-ORWELL: Tectonophysics, v. 293, p. 69–84, doi: 10.1016/S0040-1951(98)00091-2.

Greinert, J., and Nutzel, B., 2004, Hydroacoustic experiments to establish a method for the determination of methane bubble fluxes at cold seeps: Geo-Marine Letters, v. 24, p. 75–85, doi: 10.1007/s00367-003-0165-7.

Greinert, J., McGinnis, D.F., Naudts, L., Linke, P., and De Batist, M., 2010, Atmospheric methane flux from bubbling seeps: Spatially extrapolated quantification from a Black Sea shelf area: Journal of Geophysical Research, v. 115, C01002, doi: 10.1029/2009JC005381.

Grimaldo, E., Leifer, I., Gjøsund, S.H., Larsen, R.B., Larsen, T., Jeuthe, H., and Basedow, S., 2011, Field demonstration of a novel towed, area bubble-plume zooplankton (Calanus sp.) harvester: Fisheries Research, v. 107, p. 147–158, doi: 10.1016/j.fishres.2010.10.018.

Heeschen, K.U., Collier, R.W., de Angelis, M.A., Suess, E., Rehder, G., Linke, P., and Klinkhammer, G.P., 2005, Methane sources, distributions, and fluxes from cold vent sites at Hydrate Ridge, Cascadia Margin: Global Biogeochemical Cycles, v. 19, GB2016, doi: 10.1029/2004GB002266.

Hein, J.R., Normark, W.R., McIntyre, B.R., Lorenson, T.D., and Powell, C.L., II, 2006, Methanogenic calcite, ^{13}C-depleted bivalve shells, and gas hydrate from a mud volcano offshore southern California: Geology, v. 34, p. 109–112, doi: 10.1130/G22098.1.

Hickey, B.M., 1979, The California Current System—Hypothesis and facts: Progress in Oceanography, v. 8, p. 191–279, doi: 10.1016/0079-6611(79)90002-8.

Hickey, B.M., 1997, Response of a narrow submarine canyon to strong wind forcing: Journal of Physical Oceanography, v. 27, p. 697–726, doi: 10.1175/1520-0485(1997)027<0697:TROASS>2.0.CO;2.

Hickey, B.M., and Banas, N.S., 2008, Why is the northern end of the California Current System so productive?: Oceanography, v. 21, no. 4, p. 90–107.

Hornafius, J.S., Quigley, D., and Luyendyk, B.P., 1999, The world's most spectacular marine hydrocarbon seeps (Coal Oil Point, Santa Barbra Channel, California): Quantification of emissions: Journal of Geophysical Research, v. 104, no. C9, doi: 10.1029/1999JC900148.

Hovland, M., and Judd, A.G., 1988, Seabed pockmarks and seepages. Impact on geology, biology and the marine environment: London, Graham and Trotman, 293 p.

Johnson, B.D., Boudreau, B.P., Gardiner, B.S., and Maass, R., 2002, Mechanical response of sediments to bubble growth: Marine Geology, v. 187, p. 347–363, doi: 10.1016/S0025-3227(02)00383-3.

Judd, A.G., 2003, The global importance and context of methane escape from the seabed: Geo-Marine Letters, v. 23, p. 147–154, doi: 10.1007/s00367-003-0136-z.

Judd, A.G., 2004, Natural seabed gas seeps as sources of atmospheric methane: Environmental Geology, v. 46, p. 988–996, doi: 10.1007/s00254-004-1083-3.

Judd, A.G., Hovland, M., Dimitrov, L.I., Gil, S.G., and Jukes, V., 2002, The geological methane budget at continental margins and its influence on climate change: Geofluids, v. 2, p. 109–126, doi: 10.1046/j.1468-8123.2002.00027.x.

Kaartvedt, S., Melle, W., Knutsen, T., and Skjoldal, H.R., 1996, Vertical distribution of fish and krill beneath water of varying optical properties: Marine Ecology Progress Series, v. 136, p. 51–58, doi: 10.3354/meps136051.

Kvenvolden, K.A., Reeburgh, W.S., and Lorenson, T.D., 2001, Naturally occurring methane seepage, Workshop report: Eos (Transactions, American Geophysical Union), v. 82, p. 457, doi: 10.1029/01EO00275.

Leifer, I., 2010, Characteristics and scaling of bubble plumes from marine hydrocarbon seepage in the Coal Oil Point seep field: Journal of Geophysical Research, v. 115, C11014, doi: 10.1029/2009JC005844.

Leifer, I., and Boles, J., 2005, Turbine tent measurements of marine hydrocarbon seeps on subhourly timescales: Journal of Geophysical Research, v. 110, C01006, doi: 10.1029/2003JC002207.

Leifer, I., and MacDonald, I., 2003, Dynamics of the gas flux from shallow gas hydrate deposits: Interaction between oily hydrate bubbles and the oceanic environment: Earth and Planetary Science Letters, v. 210, p. 411–424, doi: 10.1016/S0012-821X(03)00173-0

Leifer, I., and Patro, R.K., 2002, The bubble mechanism for methane transport from the shallow sea bed to the surface: A review and sensitivity study: Continental Shelf Research, v. 22, p. 2409–2428, doi: 10.1016/S0278-4343(02)00065-1.

Leifer, I., Luyendyk, P., Boles, J., and Clark, J.F., 2006, Natural marine seepage blowout: Contribution to atmospheric methane: Global Biogeochemical Cycles, v. 20, doi:10.1029/2005GB002668.

Leifer, I., Jeuthe, H., Gjosund, S.H., and Johansen, V., 2009, Engineered and natural marine seep, bubble-driven buoyancy flows: Journal of Physical Oceanography, v. 39, p. 3071–3090, doi: 10.1175/2009JPO4135.1.

Lemckert, C.J., and Imberger, J., 1993, Energetic bubble plumes in arbitrary stratification: Journal of Hydraulic Engineering, v. 119, p. 680–703, doi: 10.1061/(ASCE)0733-9429(1993)119:6(680).

Martin, R.A., Nesbitt, E.A., and Campbell, K.A., 2007, Carbon stable isotopic composition of benthic foraminifera from Pliocene cold methane seeps, Cascadia accretionary margin: Palaeogeography, Palaeoclimatology, Palaeoecology, v. 246, p. 260–277, doi: 10.1016/j.palaeo.2006.10.002.

McGinnis, D.F., Greinert, J., Artemov, Y., Beaubein, S.E., and Wuest, A., 2006, Fate of rising methane bubbles in stratified waters: How much methane reaches the atmosphere?: Journal of Geophysical Research, v. 111, C09007, doi: 10.1029/2005JC003183.

McNeill, L.C., Piper, K.A., Goldfinger, C., Kulm, L.D., and Yeats, R.S., 1997, Listric normal faulting on the Cascadia continental margin: Journal of Geophysical Research, v. 102, no. B6, p. 12123–12138, doi: 10.1029/97JB00728.

Nikolovska, A., Sahling, H., and Bohrmann, G., 2008, Hydroacoustic methodology for detection, localization, and quantification of gas bubbles rising from the seafloor at gas seeps from the eastern Black Sea: Geochemistry Geophysics Geosystems, v. 9. Q10010, doi: 10.1029/2008GC002118.

Nittrouer, C.A., 1978, Detrital sediment accumulation in a continental shelf environment: An examination of the Washington shelf [Ph.D. thesis]: Seattle, Washington, University of Washington, 243 p.

Palmer, S.P., and Lingley, W.S., Jr., 1989, An assessment of the oil and gas potential of the Washington outer continental shelf: University of Washington, Washington Sea Grant Program Publication WSG89–2, 83 p.

Patro, R., Leifer, I., and Bowyer, P., 2002, Better bubble process modeling: Improved bubble hydrodynamics parameterization, *in* Donelan, M., et al., eds., Gas transfer at water surfaces: American Geophysical Union Geophysical Monograph 127, p. 315–320.

Paull, C.K., Normark, W.R., Ussler, W., III, Caress, D.W., and Keaten, R., 2008, Association among active seafloor deformation, mound formation, and gas hydrate growth and accumulation within the seafloor of the Santa Monica Basin, offshore California: Marine Geology, v. 250, p. 258–275, doi: 10.1016/j.margeo.2008.01.011.

Rasband, W., 2010, ImageJ: Bethesda, Maryland, U.S. National Institute of Health, http://rsb.info.nih.gov/ij/.

Reeburgh, W.S., 2007, Oceanic methane biogeochemistry: Chemical Reviews, v. 107, p. 486–511, doi: 10.1021/cr050362v.

Rehder, G., Leifer, I., Brewer, P.G., Friederich, G., and Peltzer, E.T., 2009, Controls on methane bubble dissolution inside and outside the hydrate stability field from open ocean field experiments and numerical modeling: Marine Chemistry, v. 114, p. 19–30, doi: 10.1016/j.marchem.2009.03.004.

Ritger, S., Carson, B., and Suess, E., 1987, Methane-derived authigenic carbonates formed by subduction-induced pore-water expulsion along the Oregon/Washington margin: Geological Society of America Bulletin, v. 98, p. 147–156, doi: 10.1130/0016-7606(1987)98<147:MACFBS>2.0.CO;2.

Sameoto, D.D., 1982, Zooplankton and micronekton abundance in acoustic scattering layers on the Nova Scotian slope: Canadian Journal of Fisheries and Aquatic Sciences, v. 39, p. 760–777, doi: 10.1139/f82-104.

Sauter, E.J., Muyakshin, S.L., Charlou, J., Schluter, M., Boetius, A., Jerosch, K., Damm, E., Foucher, J., and Klages, M., 2006, Methane discharge from a deep-sea submarine mud volcano into the upper water column by gas hydrate-coated methane bubbles: Earth and Planetary Science Letters, v. 243, p. 354–365, doi: 10.1016/j.epsl.2006.01.041.

Schladow, S.G., 1993, Lake destratification by bubble-plume systems: Design methodology: Journal of Hydraulic Engineering, v. 119, p. 350–368, doi: 10.1061/(ASCE)0733-9429(1993)119:3(350).

Sevadjian, J.C., McManus, M.A., and Pawlak, G., 2010, Effects of physical structure and processes on thin zooplankton layers in Mamala Bay, Hawaii: Marine Ecology Progress Series, v. 409, p. 95–106, doi: 10.3354/meps08614.

Silver, E.A., 1972, Pleistocene tectonic accretion of the continental slope off Washington: Marine Geology, v. 13, p. 239–249, doi: 10.1016/0025-3227(72)90053-9.

Solomon, S., Qin, D., Manning, M., Chen, Z., Marquis, M., Averyt, K.B., Tignor, M., and Miller, H.L., Jr., eds., 2007, Climate change 2007: The physical science basis. Contribution of Working Group I to the Fourth Assessment Report of the Intergovernmental Panel on Climate Change: Cambridge, UK, Cambridge University Press, 989 p.

Stanton, T.K., Chu, D., and Wiebe, P.H., 1996, Acoustic scattering characteristics of several zooplankton groups: ICES Journal of Marine Science, v. 53, p. 289–295, doi: 10.1006/jmsc.1996.0037.

Sternberg, R.W., 1986, Transport and accumulation of river-derived sediment on the Washington continental shelf, USA: Geological Society of London Journal, v. 143, p. 945–956, doi: 10.1144/gsjgs.143.6.0945.

Suess, E., and 19 others, 2001, Sea floor methane hydrates at Hydrate Ridge, Cascadia Margin, *in* Paull, C., and Dillon, W.P., eds., Natural gas hydrates: Occurrence, distribution, and detection: American Geophysical Union Geophysical Monograph 124, p. 87–98.

Thomson, R.E., and Allen, S.E., 2000, Time series acoustic observations of macrozooplankton diel migration and associated pelagic fish abundance: Canadian Journal of Fisheries and Aquatic Sciences, v. 57, p. 1919–1931, doi: 10.1139/f00-142.

Torres, M.E., Embley, R.W., Merle, S.G., Trehu, A.M., Collier, R.W., Suess, E., and Heeschen, K.U., 2009, Methane sources feeding cold seeps on the shelf and upper continental slope off central Oregon, USA: Geochemistry Geophysics Geosystems, v. 10, no. 11, Q11003, doi: 10.1029/2009GC002518.

Tryon, M.D., Brown, K.M., and Torres, M.E., 2002, Fluid and chemical flux in and out of sediments hosting methane hydrate deposits on Hydrate Ridge, OR, II: Hydrological processes: Earth and Planetary Science Letters, v. 201, p. 541–557, doi: 10.1016/S0012-821X(02)00732-X.

Zutic, V.B., Cosovic, B., Marcenko, E., and Bihari, N., 1981, Surfactant production by marine phytoplankton: Marine Chemistry, v. 10, p. 505–520, doi: 10.1016/0304-4203(81)90004-9.

Manuscript Received 6 October 2010
Revised Manuscript Received 25 May 2011
Manuscript Accepted 8 July 2011